# The formation of dip and peak structures for the kurtosis of net baryon number fluctuations along the freeze-out line

Zhibin Li <sup>a,b</sup>, Xinyang Wang<sup>a</sup>, and Mei Huang<sup>a,b,c</sup>

<sup>a</sup> Institute of High Energy Physics, Chinese Academy of Sciences, Beijing 100049, China

<sup>b</sup> School of Physics Sciences, University of Chinese Academy of Sciences, Beijing 100039, China and

<sup>c</sup> Theoretical Physics Center for Science Facilities,

Chinese Academy of Sciences, Beijing 100049, China

We analyze the structure of the kurtosis  $\kappa\sigma^2$  of net baryon number fluctuation along the freeze out line and discuss the signature of the existence of the QCD critical end point (CEP) in the NJL model, PNJL model as well as  $\mu$ PNJL model with different parameter sets. It is found that at zero chemical potential, the main contribution to the baryon number fluctuation comes from gluodynamics, and the temperature dependent  $\kappa\sigma^2$  can be used to constrain the model. The peak structure of  $\kappa\sigma^2$  along the freeze-out line is solely determined by the existence of the CEP mountain and can be used as a clean signature for the existence of CEP. The formation of the dip structure is sensitive to the relation between the freeze-out line and the phase boundary. The dip structure can be formed if the freeze-out line starts from the temperature above the critical temperature at  $\mu=0$  and crosses the foot of the CEP mountain. It is noticed that the extracted freeze-out temperature from beam energy scan measurement at RHIC is indeed higher than the crossover phase boundary, which supports our analysis for the formation of the dip structure. Around the CEP for chiral phase transition there is a negative region of  $\kappa\sigma^2$  from the crossover side, the positive  $\kappa\sigma^2$  at the dip from measurement indicates that the freeze-out line is away from the negative region.

PACS numbers: 12.38.Mh,25.75.Nq,11.10.Wx,11.25.Tq

#### I. INTRODUCTION

The phase transition and phase structure of Quantum Chromodynamics (QCD) under extreme conditions is the main topic of relativistic heavy ion collisions, and it is also highly related to the evolution of the early universe and the equation of state inside the compact stars. Lattice QCD calculation shows that at small baryon density, the QCD phase transitions including the chiral phase transition as well as deconfinement phase transition are of crossover at finite temperature [1–3]. From symmetry analysis and effective chiral models, it is generally believed that at high baryon density the chiral phase transition is of first order and there exists a QCD critical end point (CEP) for chiral phase transition in the temperature and baryon chemical potential plane [4–23]. The QCD CEP have been widely analyzed in different models, e.g., Nambu–Jona-Lasinio (NJL) model, the Polyakov-loop improved NJL (PNJL) model, linear sigma model, quark-meson (QM) model, the Polyakov-loop improved QM model, the Dyson-Schwinger equations (DSE), and the holographic QCD model [6–19, 24]. However, different models even the same model with different parameter sets give various location of CEP[25]. Therefore, to search for the existence of the CEP and further to locate the CEP is one of the most central goals at Relativistic Heavy Ion Collisions (RHIC) as well as for the future accelerator facilities at Facility for Antiproton and Ion Research (FAIR) in Darmstadt and Nuclotron-based Ion Collider Facility (NICA) in Dubna.

The cumulants of conserved quantities up to fourth order of net-proton, net-charge and net-kaon multiplicity distributions have been measured in the first phase of beam energy scan program (BES-I) at RHIC for Au+Au collisions at  $\sqrt{s_{NN}}=7.7,11.5,14.5,19.6,27,39,62.4$  and 200GeV, and the results are summarized in [26–28]. A non-monotonic energy dependent behavior for the kurtosis of the net proton number distributions  $\kappa\sigma^2$  has been observed in the most central Au+Au collisions:  $\kappa\sigma^2$  firstly decreases from around 1 at the colliding energy  $\sqrt{s_{NN}}=200{\rm GeV}$  to 0.1 at  $\sqrt{s_{NN}}=20{\rm GeV}$  and then rises quickly up to around 3.5 at  $\sqrt{s_{NN}}=7{\rm GeV}$ . The second phase of beam energy scan (BES-II) at RHIC will be performed in 2019-2020, therefore it is very urgent for both experimentalists and theorists to extract a clean signature to identify the existence of the QCD CEP and further to locate the CEP. On the one hand, we should try to extract useful information about QCD phase transitions from the measurement along the freeze out line, and to find the evidence of the QCD CEP. On the other hand, we should explore carefully how QCD phase transitions will shed light on properties of the cumulants of conserved quantities at freeze-out, and we have to understand: 1) The large magnitude of  $\kappa\sigma^2 \sim 1$  at zero chemical potential; 2) The decreasing tendency of  $\kappa\sigma^2$  in the collision energy period of  $200 \sim 20{\rm GeV}$ ; 3) The rising of  $\kappa\sigma^2$  in the collision energy period of  $20 \sim 7{\rm GeV}$ . We have to also predict the behavior of  $\kappa\sigma^2$  below the collision energy 7GeV.

By using the Ising model, it was pointed out in [21] that the quartic cumulant (or kurtosis) of the order parameter is universally negative when the critical point is approaching to the crossover side of the phase separation line. From the results in [21], the oscillation behavior of the kurtosis along the freeze out line has been regarded as a typical

signature of the existence of the CEP. Many interests have focused on the sign changing of various cumulants around the CEP, and the sign changing for higher order susceptibilities has been recently discussed in [11]. It is noticed that the sign changing for the 6th and 8th order susceptibilities starts at the baryon chemical potential quite far away from the CEP, it may indicate that the sign changing of cumulans of conserved quantities is not directly related to the CEP. In the holographic QCD model [29], we explained that the sign changing of the baryon number susceptibilities along the freeze-out line is not necessarily related to the CEP, but the peaked baryon number susceptibilities along the freeze-out line is solely determined by the CEP thus can be used as an evident signature for the existence of the CEP, and the peak position is close to the location of the CEP in the QCD phase diagram. Furthermore, it is found that at zero chemical potential, the magnitude of  $\kappa\sigma^2$  around the phase transition line in the gluodynamics dominant holographic QCD model is around 1, which is in agreement with lattice result, and is much larger than that in the Ising model (close to zero), and also much larger than that in the NJL model (around 0.1). Therefore, it is natural to speculate that the gluodynamics contribution is dominant to the baryon number susceptibilities, which is quite surprising!

In order to check the gluodynamics contribution to the baryon number susceptibilities, in this work, we will try to explore the structure of the kurtosis of the net proton number distribution  $\kappa\sigma^2$  along the freeze out line in the Nambu–Jona-Lasinio (NJL) model, the Polyakov-loop improved NJL (PNJL) model as well as  $\mu$ -dependent Polyakov-loop potential improved NJL ( $\mu$ PNJL) model. Also in order to investigate the relation between the CEP and the structure of the  $\kappa\sigma^2$  along the freeze out line, we will need to shift the location of the CEP by introducing the interaction in the vector channel. This paper is organized as following: in the next section, we give a brief introduction to the two-flavor NJL model, the Polyakov-loop improved NJL (PNJL) model as well as  $\mu$  Polyakov-loop improved NJL ( $\mu$ PNJL) model. In Sec. III we show numerical results and analysis. Finally, the discussion and conclusion part is given in Sec. IV.

#### II. THE MODELS

We will investigate the gluodynamics contribution to the kurtosis of the net proton number distribution  $\kappa\sigma^2$ , therefore we will compare  $\kappa\sigma^2$  in the framework of NJL model, the Polyakov-loop improved NJL (PNJL) model as well as NJL with  $\mu$ -dependent Polyakov-loop potential ( $\mu$ PNJL) model, and analyze the structure of  $\kappa\sigma^2$  along the freeze out line and its relation with the existence and location of the QCD CEP.

#### A. The NJL model with vector interaction

In order to shift the location of the CEP, we introduce the two-flavor NJL model with the vector interaction, and the Lagrangian is given by [30–32]

$$\mathcal{L}_{\text{NJL}} = \bar{\psi}(i\gamma_{\mu}\partial^{\mu} - m)\psi + G_{S}[(\bar{\psi}\psi)^{2} + (\bar{\psi}i\gamma_{5}\vec{\tau}\psi)^{2}] - G_{V}[(\bar{\psi}\gamma_{\mu}\psi)^{2} + (\bar{\psi}\gamma_{\mu}\gamma_{5}\psi)^{2}]. \tag{1}$$

Where  $\psi = (u, d)^T$  is the doublet of the two light quark flavors u and d with the current mass  $m = m_u = m_d$ , and  $\vec{\tau} = (\tau^1, \tau^2, \tau^3)$  the isospin Pauli matrix.  $G_S$  and  $G_V$  are the coupling constants in the (psudo)scalar channel and the vector channel, respectively. By introducing the auxiliary fields for scalars and vectors, and in the vacuum we take the mean-field approximation with

$$\sigma_i = \langle \bar{\psi}_i \psi_i \rangle, \quad \rho_i = \langle \psi_i^{\dagger} \psi_i \rangle,$$
 (2)

the quark condensate and the net quark number density of flavor i respectively. Then the thermodynamical potential of this NJL model takes the following form:

$$\Omega_{\text{NJL}} = -2N_c \sum_{i=u,d} \int_0^{\Lambda} \frac{d^3p}{(2\pi)^3} \left[ E_i + T \ln(1 + e^{-\beta(E_i - \tilde{\mu}_i)}) + T \ln(1 + e^{-\beta(E_i + \tilde{\mu}_i)}) \right] + G_S(\sigma_u + \sigma_d)^2 - G_V(\rho_u + \rho_d)^2, \quad (3)$$

with  $N_c = 3$  the number of colors. The quark quasiparticle energies  $E_i$  and constituent quark masses  $M_i$  for flavors i = (u, d) are given by

$$E_i = \sqrt{p^2 + M_i^2}, \quad M_i = m_i - 2G_S(\sigma_u + \sigma_d),$$
 (4)

and the effective chemical potentials are shifted by

$$\tilde{\mu}_i = \mu_i - 4G_V \rho_i. \tag{5}$$

In order to solve the minimum of the thermal potential  $\Omega_{\rm NJL}$ , we have the following gap equations

$$\frac{\partial \Omega_{NJL}}{\partial \sigma_{u}} = \frac{\partial \Omega_{NJL}}{\partial \sigma_{d}} = 0, \tag{6}$$

and

$$\rho_i = -\frac{\partial \Omega_{NJL}}{\partial \mu_i}. (7)$$

## B. The PNJL and $\mu$ PNJL Model

In the 2-flavor PNJL and  $\mu$ PNJL models, we need to add the Polyakov-loop effective potential  $\mathcal{U}(\Phi, \bar{\Phi}, T)$  with the following ansatz [33–36]

$$\frac{\mathcal{U}(\Phi, \bar{\Phi}, T)}{T^4} = -\frac{a(T)}{2}\bar{\Phi}\Phi + b(T)\ln[1 - 6\bar{\Phi}\Phi + 4(\bar{\Phi}^3 + \Phi^3) - 3(\bar{\Phi}\Phi)^2],\tag{8}$$

where  $a(T) = a_0 + a_1(\frac{T_0}{T}) + a_2(\frac{T_0}{T})^2$  and  $b(T) = b_3(\frac{T_0}{T})^3$ . The critical temperature of the confinement-deconfinement phase transition  $T_0$  in pure gluon system is 270MeV, and we rescale  $T_0$  to 200MeV because of the presence of fermion fields. The thermodynamical potential of this PNJL model is given by

$$\Omega_{PNJL} = \mathcal{U}(\Phi, \bar{\Phi}, T) - 2N_c \sum_{i=u,d} \int_0^{\Lambda} \frac{d^3p}{(2\pi)^3} [E_i] + G_S(\sigma_u + \sigma_d)^2 - G_V(\rho_u + \rho_d)^2 
-2T \sum_{i=u,d} \int_0^{\Lambda} \frac{d^3p}{(2\pi)^3} [\ln(1 + 3\Phi e^{-\beta(E_i - \tilde{\mu}_i)} + 3\bar{\Phi}e^{-2\beta(E_i - \tilde{\mu}_i)} + e^{-3\beta(E_i - \tilde{\mu}_i)})] 
-2T \sum_{i=u,d} \int_0^{\Lambda} \frac{d^3p}{(2\pi)^3} [\ln(1 + 3\bar{\Phi}e^{-\beta(E_i + \tilde{\mu}_i)} + 3\Phi e^{-2\beta(E_i + \tilde{\mu}_i)} + e^{-3\beta(E_i + \tilde{\mu}_i)})]$$
(9)

with the same definitions of  $E_i$ ,  $M_i$  and  $\tilde{\mu}_i$  as in the NJL model. The gap equations are determined by

$$\frac{\partial \Omega_{PNJL}}{\partial \sigma_u} = \frac{\partial \Omega_{PNJL}}{\partial \sigma_d} = \frac{\partial \Omega_{PNJL}}{\partial \Phi} = \frac{\partial \Omega_{PNJL}}{\partial \bar{\Phi}} = 0, \tag{10}$$

and

$$\rho_i = -\frac{\partial \Omega_{PNJL}}{\partial \mu_i}. (11)$$

By considering the back-reaction of quark to the glue sector, we take the so called  $\mu$ PNJL model with the  $\mu$ -dependent  $T_0[37–39]$ 

$$T_0(N_f, \mu_i) = T_\tau e^{-\frac{1}{\alpha_0 f(N_f, \mu_i)}}$$
(12)

where  $f(N_f, \mu_i) = \frac{11N_c - 2N_f}{6\pi} - \kappa \frac{16N_f}{\pi} \frac{\mu^2}{T_\tau^2}$  and  $\mu = \frac{1}{N_f} \sum_i \mu_i$ . The thermodynamical potential of  $\mu$ PNJL model  $\Omega_{\mu}$ PNJL has the same form of PNJL model, and the gap equations take the following form:

$$\frac{\Omega_{\mu \text{PNJL}}}{\partial \sigma_u} = \frac{\partial \Omega_{\mu \text{PNJL}}}{\partial \sigma_d} = \frac{\partial \Omega_{\mu \text{PNJL}}}{\partial \Phi} = \frac{\partial \Omega_{\mu \text{PNJL}}}{\partial \bar{\Phi}} = 0, \tag{13}$$

and

$$\rho_i = -\frac{\partial \Omega_{\mu \text{PNJL}}}{\partial \mu_i}.$$
 (14)

#### C. The definition of kurtosis

BES-I measures the baryon number susceptibilities, which are defined as the derivative of the dimensionless pressure with respected to the reduced chemical potential [28]

$$\chi_n^B = \frac{\partial^n [P/T^4]}{\partial [\mu_B/T]^n},\tag{15}$$

with the pressure  $P = -\Omega$  which is just the minus thermodynamical potential. The cumulants of baryon number distributions are given by

$$C_n^B = VT^3 \chi_n^B. (16)$$

By introducing the variance  $\sigma^2 = C_2^B$ , kurtosis  $\kappa = \frac{C_4^B}{(\sigma^2)^2}$ , one can have the following relation between observable quantities and theoretical calculations:

$$\kappa \sigma^2 = \frac{C_4^B}{C_2^B} = \frac{\chi_4^B}{\chi_2^B},\tag{17}$$

which relates  $\kappa\sigma^2$  with the ratio of fourth and second order cumulants of net-baryon number fluctuations.

#### III. NUMERICAL RESULTS

#### A. Parameter sets and the location of CEP

For numerical calculations, we fix  $m_u = m_d = 5.5 \text{MeV}, N_c = 3, N_f = 2 \text{ in all the models}.$ 

In the regular NJL model, we choose the parameters as in Ref.[40]:  $\Lambda=651 {\rm MeV}, G_S=5.04 {\rm GeV}^{-2}$ . To shift the location of the CEP in the NJL model we choose different coupling constant in the vector channel:  $G_V=-0.5G_S$ ,  $G_V=0$  and  $G_V=0.67G_S$  [11], which is indicated as NJL-1, NJL-2, NJL-3 respectively. Correspondingly, the locations of CEP in NJL-1 and NJL-2 are ( $\mu_B^c=796.7 {\rm MeV}, T^c=76.8 {\rm MeV}$ ), ( $\mu_B^c=1005.2 {\rm MeV}, T^c=34.6 {\rm MeV}$ ), respectively, there is no CEP in NJL-3.

In the PNJL model, we fix  $T_0=200 {\rm MeV}$ , and choose three different parameter sets for numerical calculations. The PNJL-1 is defined by using the following parameters:  $a_0=3.51,\ a_1=-2.47,\ a_2=14.5,\ b_3=-1.95$  and  $\Lambda=648 {\rm MeV},\ G_S=4.98 {\rm GeV}^{-2},\ G_V=-0.35 G_S$ . At  $\mu=0$ , the critical temperature for the chiral phase transition is  $T_0^\chi=203.4 {\rm MeV}$ , and for deconfinement phase transition is  $T_0^D=191.2 {\rm MeV}$ , and the CEP is located at  $(\mu_B^c=778.2 {\rm MeV},T^c=149.1 {\rm MeV})$ . For the PNJL-2, we choose the parameters:  $a_0=3.51,\ a_1=-2.47,\ a_2=15.2,\ b_3=-1.75$  for the Polyakov loop potential part and  $\Lambda=651 {\rm MeV},\ G_S=5.04 {\rm GeV}^{-2},\ G_V=0$  for the quark interaction part. At  $\mu=0$ , the critical temperature for the chiral phase transition is  $T_0^\Delta=201.5 {\rm MeV}$ , and for deconfinement phase transition is  $T_0^D=185.6 {\rm MeV}$ , and the CEP is located at  $(\mu_B^c=971.5 {\rm MeV},T^c=103.2 {\rm MeV})$ . The parameter set of PNJL-3 is given by:  $a_0=3.51,\ a_1=-2.47,\ a_2=15.2,\ b_3=-1.75$  and  $\Lambda=651 {\rm MeV},\ G_S=5.04 {\rm GeV}^{-2},\ G_V=0.67 G_S$ . At  $\mu=0$ , the critical temperature for the chiral phase transition is  $T_0^\Delta=202.3 {\rm MeV}$ , and for deconfinement phase transition is  $T_0^D=185.8 {\rm MeV}$ , and there is no CEP in the PNJL Model-3.

In the  $\mu$ PNJL model, we choose two different parameter sets. For  $\mu$ PNJL-1, we have the parameters:  $T_{\tau}=1770 \, \mathrm{MeV}$ ,  $\alpha_0=0.304$ ,  $\kappa=0.2$ ,  $a_0=3.51$ ,  $a_1=-2.47$ ,  $a_2=15.2$ ,  $b_3=-1.75$  and  $\Lambda=651 \, \mathrm{MeV}$ ,  $G_S=5.04 \, \mathrm{GeV}^{-2}$ . With this parameter set, at  $\mu=0$ , the critical temperature for the chiral phase transition is  $T_0^{\chi}=204.9 \, \mathrm{MeV}$ , and for deconfinement phase transition is  $T_0^D=170.4 \, \mathrm{MeV}$ , and the CEP is located at ( $\mu_B^c=983.5 \, \mathrm{MeV}$ ,  $T^c=82.0 \, \mathrm{MeV}$ ). For  $\mu$ PNJL-2, we have the parameters:  $T_{\tau}=1870 \, \mathrm{MeV}$ ,  $\alpha_0=0.304$ ,  $\kappa=0.2$ ,  $a_0=3.51$ ,  $a_1=-2.47$ ,  $a_2=14.5$ ,  $b_3=-1.95$  and  $\Lambda=648 \, \mathrm{MeV}$ ,  $G_S=4.98 \, \mathrm{GeV}^{-2}$ , with the location of CEP at ( $\mu_B^c=967.8 \, \mathrm{MeV}$ ,  $T^c=63.9 \, \mathrm{MeV}$ ), and at  $\mu=0$ , the critical temperature for the chiral phase transition is  $T_0^{\chi}=212.1 \, \mathrm{MeV}$ , and for deconfinement phase transition is  $T_0^D=194.3 \, \mathrm{MeV}$ .

# B. The gluodynamics contribution to $\kappa \sigma^2$

In Fig.1, we show  $\kappa\sigma^2$  as a function of  $T/T_0$  in three parameter sets of NJL model, and three parameter sets of PNJL model and two parameter sets of  $\mu$ PNJL model at zero chemical potential, and compare with lattice results in [41], with  $T_0$  the critical temperature for chiral phase transition at zero chemical potential  $\mu_B = 0$ . The critical

temperature of lattice data at  $\mu=0$  is  $154\pm9 \mathrm{MeV}$  and we choose 156MeV. The value of  $\kappa\sigma^2$  of net baryon number fluctuations is unity in the limit of hadron resonance gas (HRG) and, in the ideal free quark gas (FQG) limit at infinite temperature it takes the value of  $\kappa\sigma^2\simeq0.068$ , which are also shown in Fig.1. It is worthy of mentioning that from the lattice result shown in Ref.[41], that at the critical temperature  $T_0$ , the magnitude of  $\kappa\sigma^2$  is around 0.8, which is smaller than its value of 1 at the temperature of  $T_0^{dec}\simeq140 \mathrm{MeV}$ , at which quark matter transfers to hadron gas. Here  $T_0^{dec}$  describes a physical "confinement-deconfinement" transition, which is different from the  $T_0^D$  describing the confinement-deconfinement phase transition by using the order parameter of Polyakov loop.

In the NJL model, the magnitude of  $\kappa \sigma^2$  at  $T_0$  is around 0.4, 0.2, 0.1 in the NJL-1, NJL-2 and NJL-3, which is much smaller than the lattice result. In the whole temperature region  $T > T_0$ , the magnitude of  $\kappa \sigma^2$  is quite small comparing with the lattice results.

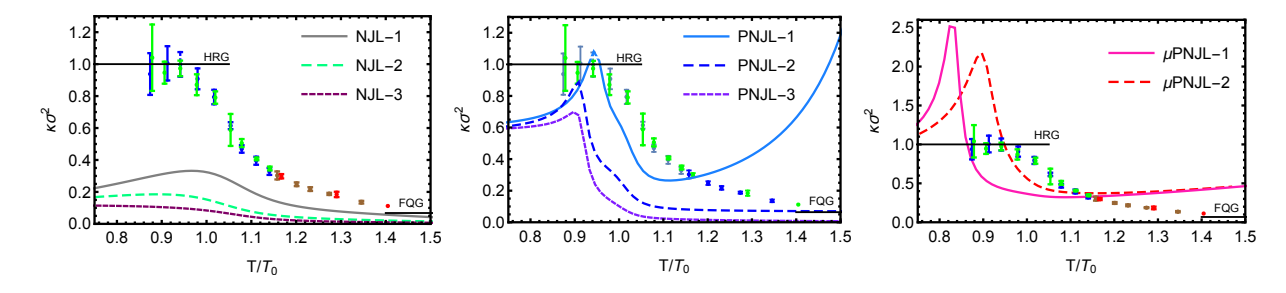


FIG. 1: The kurtosis of baryon number fluctuation  $\kappa\sigma^2$  as a function of the temperature at zero baryon number density in the NJL model, PNJL model and  $\mu$ PNJL model, and compare with the lattice result in [41].  $\kappa\sigma^2 = 1$  in the hadron resonance gas (HRG) limit and  $\kappa\sigma^2 \simeq 0.068$  in the ideal free quark gas (FQG) limit.

When the gluodynamics contribution is taken into account in the PNJL model, the critical temperatures for the chiral phase transition  $T_0^X$  and deconfinement phase transition  $T_0^D$  are separated, and the critical temperature for the deconfinement phase transition  $T_0^X$  is lower than that of the chiral phase transition  $T_0^X$  at zero chemical potential. It is observed that the magnitude of  $\kappa\sigma^2$  shows a peak at the critical temperature for deconfinement phase transition  $T_0^D$ , and in the hadron gas phase with  $T < T_0^D$ , the magnitude of  $\kappa\sigma^2$  decreases with the decreasing temperature, and smaller than the HRG limit. With the parameter sets used in the PNJL-1, the peak value of  $\kappa\sigma^2$  can reach 1 at  $T_0^D$ , and is around 0.8 at  $T_0^X$ , which is in agreement with the lattice result. However, with a negative coupling constant in the vector channel  $G_V = -0.35G_S$ , the magnitude of  $\kappa\sigma^2$  at high temperature is obviously not correct, it does not decrease to the free gas limit but increases rapidly when  $T > 1.1T_0^X$  and rise up again to 1 at around  $T = 1.5T_0^X$ . However, in this work, we only need the information of the model around phase transition and its location of CEP, we can still use the parameter set in PNJL-1.

For the  $\mu$ PNJL model, the magnitude of  $\kappa\sigma^2$  also shows a peak at the critical temperature of deconfinement phase transition  $T_0^D$ . However, the peak value is around 2 and much larger than the lattice result. In the region of  $T>1.1T_0$ , the magnitude of  $\kappa\sigma^2$  does not decreases to the free quark gas limit but increases with the temperature and is larger than lattice result. This indicate that the  $\mu$  dependent Polyakov-loop potential is not properly added, which can be improved in the future.

From the magnitude of  $\kappa \sigma^2$  in the NJL model, PNJL model and  $\mu$ PNJL model, we can see that the dominant contribution to  $\kappa \sigma^2$  comes from gluodynamics at zero chemical potential. In the future for model construction,  $\kappa \sigma^2$  as a function of the temperature can be used to constrain models.

## C. The kurtosis of baryon number fluctuation $\kappa \sigma^2$ in the NJL model

In Fig. 2, we show the 3D plot for the kurtosis of baryon number fluctuation  $\kappa\sigma^2$  as a function of the temperature and baryon chemical potential in the NJL model. In Fig.3 we show the chiral phase transition line and 2D plot for  $\kappa\sigma^2$  as a function of the baryon chemical potential along different freeze-out lines for NJL-1,NJL-2 and NJL-3, respectively.

By changing the coupling constant in the vector channel, the location of the CEP will shift. The CEP in the NJL-1 and NJL-2 is located at ( $\mu_B^c = 796.7 \text{MeV}$ ,  $T^c = 76.8 \text{MeV}$ ), ( $\mu_B^c = 1005.2 \text{MeV}$ ,  $T^c = 34.6 \text{MeV}$ ), respectively, and it is observed that  $\kappa \sigma^2$  develops a high CEP mountain in the NJL-1 and NJL-2. There is no CEP in the NJL-3, therefore, no CEP mountain of  $\kappa \sigma^2$  develops in the NJL-3. From the 3D plot in Fig. 2, one can observe an obvious chiral phase boundary in the crossover side, and the magnitude of its ridge decreases with the increase of the baryon chemical potential. Here we define the ridge as along the phase boundary, the back/front ridge as the higher/lower

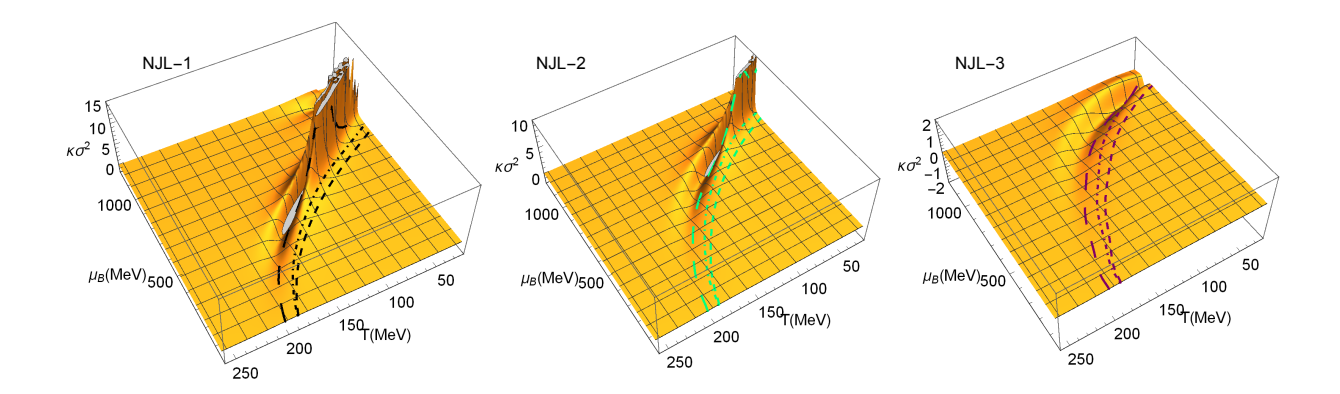


FIG. 2: The 3D plot for the kurtosis of the baryon number fluctuation  $\kappa \sigma^2$  as a function of the temperature and baryon chemical potential in the NJL model.

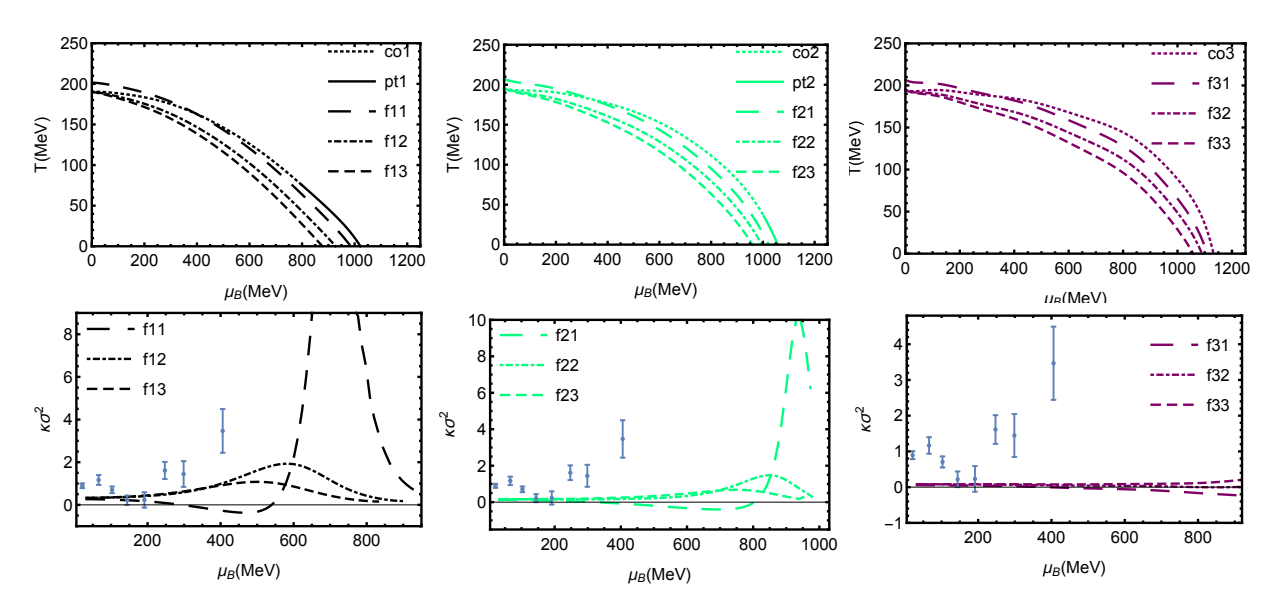


FIG. 3: (Above) The chiral phase transition line in the NJL model and three different freeze-out lines:1) Starting from the back ridge of the chiral phase boundary, goes through the negative region and then cross the phase boundary; 2) Starting from the front ridge of the chiral phase boundary and then cross the foot of the CEP mountain; 3) Far away from the phase boundary. These three free-out lines are indicated by long dashed, dashed-dotted and dashed lines, respectively. (Below) The 2D plot for  $\kappa\sigma^2$  as a function of the baryon chemical potential along three freeze-out lines and comparing with BES-I measurement.

temperature side comparing with the phase boundary, respectively. If there is a CEP located on the phase diagram, a CEP mountain rises up around the CEP, and one can observe a negative region of  $\kappa\sigma^2$  around the CEP above the chiral phase boundary extended from the crossover side.

Because the measurement of heavy-ion collision is along the freeze-out line, we choose three different freeze-out lines in the NJL model: 1) Starting from the back ridge of the chiral phase boundary, goes through the negative region and then cross the phase boundary; 2) Starting from the front ridge of the chiral phase boundary and then cross the foot of the CEP mountain; 3) Far away from the phase boundary. These three free-out lines are indicated by long dashed, dashed-dotted and dashed lines, respectively.

It is observed that when the freeze-out line crosses the CEP mountain or crosses the foot of the CEP mountain, there will be a peak showing up for  $\kappa\sigma^2$  along the freeze-out line, and the location of the peak is close to the location of the CEP mountain. In the case of no CEP, it is found that  $\kappa\sigma^2$  keeps flat in almost the whole region and does not show any structure. The BES-I measurement is also shown in the 2D plot of  $\kappa\sigma^2$  as a function of the baryon chemical potential for comparing. In the NJL-1 and NJL-2 with the existence of CEP in the phase diagram, it is found that for the first case freeze-out line, because the freeze-out line starts from the back ridge of the chiral phase boundary and goes through the negative region of  $\kappa\sigma^2$ , then crosses the CEP mountain, therefore,  $\kappa\sigma^2$  decreases from around 0.1

and then down to negative value then rises up quickly and shows up a high peak around the critical chemical potential, which shows a dip and then a peak structure of  $\kappa\sigma^2$  along the freeze-out line. For the second case of freeze-out line, because the freeze-out line starts from the front ridge of the chiral phase boundary, and then crosses the foot of the CEP mountain, we can only see a peak structure of  $\kappa\sigma^2$  along the freeze-out line at high chemical potential. For the third case of freeze-out, if the freeze-out line is far away from the phase boundary, one can only observe a weak peak of  $\kappa\sigma^2$  along the freeze-out line.

It is found that the magnitude of  $\kappa \sigma^2$  in the NJL model at small baryon chemical potential region is small comparing with experiment measurement.

# D. The kurtosis of the baryon number fluctuation $\kappa \sigma^2$ in the PNJL model

In Fig. 4, we show the 3D plot for the kurtosis of baryon number fluctuation  $\kappa\sigma^2$  as a function of the temperature and baryon chemical potential in the PNJL model. In Fig.5 we show the phase transition lines and 2D plot for  $\kappa\sigma^2$  as a function of the baryon chemical potential along different freeze-out lines for PNJL-1,PNJL-2 and PNJL-3, respectively.

Different from the NJL model, in the PNJL model, when the gluodynamics is taken into account, there will be two phase transitions: one for the chiral phase transition and another for the deconfinement phase transition, and the deconfinement phase transition line lays below the chiral phase transition line at small chemical potential region. The two separate phase transition lines can be obviously seen from the  $(T, \mu)$  phase diagram in Fig.5. In the 3D plot Fig.4 one can observe two separate phase boundaries at small baryon chemical potentials, and a valley forms in between the two phase boundaries. It is noticed that the magnitude of baryon number fluctuation  $\kappa\sigma^2$  is quite small along the chiral phase boundary, but around 1 along the deconfinement phase boundary.

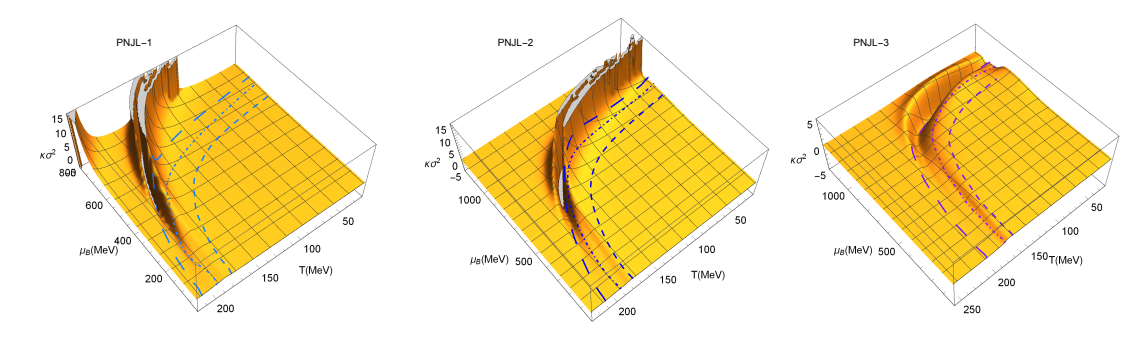


FIG. 4: The 3D plot for the kurtosis of baryon number fluctuation  $\kappa \sigma^2$  as a function of the temperature and baryon chemical potential in the PNJL model.

By changing the coupling constant in the vector channel and parameter sets, the CEP of the chiral phase transition in the PNJL model can shift. The CEPs are located at ( $\mu_B^c = 778.2 \text{MeV}$ ,  $T^c = 149.1 \text{MeV}$ ) and ( $\mu_B^c = 971.5 \text{MeV}$ ,  $T^c = 103.2 \text{MeV}$ ) in the PNJL-1 and PNJL-2 models, respectively. Even though the two critical baryon chemical potentials  $\mu_B^c$  in the PNJL-1 and PNJL-2 are almost the same, the critical temperature in the PNJL-1 model is higher than that in the PNJL-2. For the parameters used in the PNJL-3, there is no CEP shows up in the phase diagram. From the 3D plot in Fig. 4, one can observe two obvious phase boundaries for the chiral and deconfinement phase transitions in the crossover side, and the magnitude of the deconfinement ridge is much higher than the chiral ridge. If a CEP for the chiral phase transition exists in the PNJL model, the structure of the CEP mountain for the chiral phase transition looks as the same as that in the NJL model, and one can observe a negative region of  $\kappa \sigma^2$  around the CEP above the chiral phase boundary extended from the crossover side. The only difference is that the deconfinement phase boundary extends to the CEP mountain and merges with the chiral phase boundary.

The structure of  $\kappa\sigma^2$  along the freeze-out line in the PNJL model is more complicated due to the two separated phase boundaries. Comparing with the NJL model, the magnitude of  $\kappa\sigma^2$  at small baryon chemical potentials in the PNJL model is in agreement with experiment measurement due to the contribution from gluodynamics. We also choose three different freeze-out lines: 1) Starting from the back ridge of the chiral phase boundary, goes through the negative region and then crosses the foot of the CEP mountain; 2) Starting from the back ridge of the deconfinement phase boundary, and then crosses the foot of the CEP mountain; 3) Starting from the front ridge of the deconfinement phase boundary and keeps far away from the CEP mountain. These three different freeze-out lines are indicated by long dashed, dashed-dotted and dashed lines, respectively. Here the back/ front ridge also means the higher/lower temperature side comparing with the phase boundary, respectively.

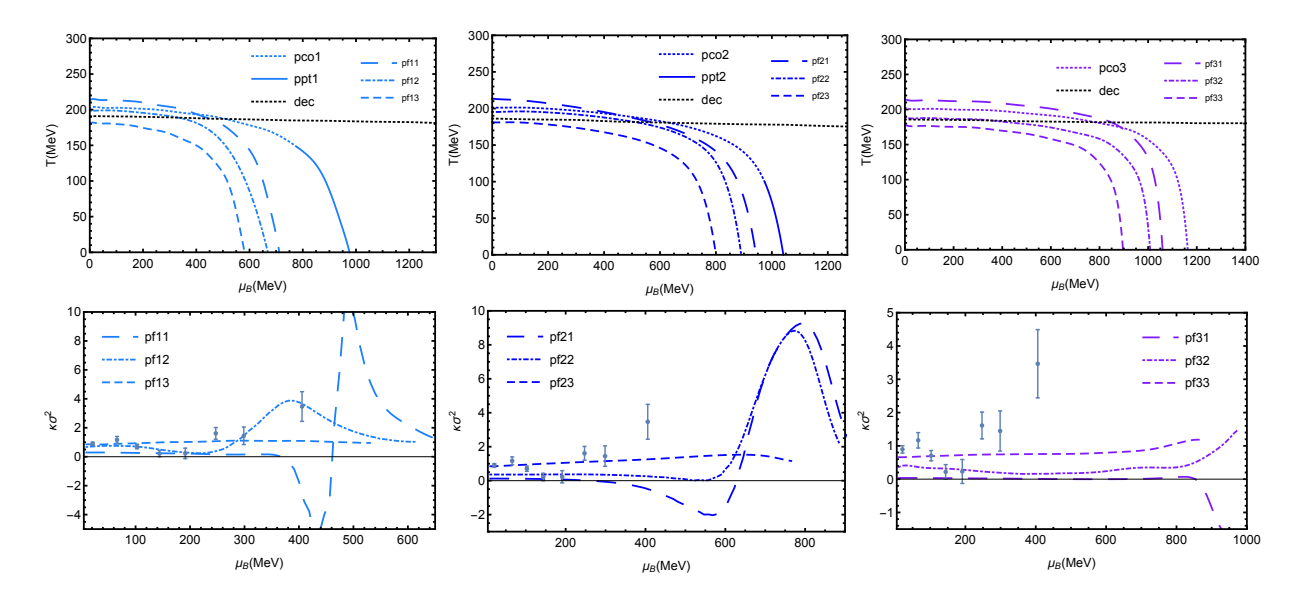


FIG. 5: (Above) The chiral phase transition line in the PNJL model and three different freeze-out lines: 1) Starting from the back ridge of the chiral phase boundary, goes through the negative region and then crosses the foot of the CEP mountain; 2) Starting from the back ridge of the deconfinement phase boundary, and then crosses the foot of the CEP mountain; 3) Starting from the front ridge of the deconfinement phase boundary and keeps far away from the CEP mountain. These three different freeze-out lines are indicated by long dashed, dashed-dotted and dashed lines, respectively. (Below) The 2D plot for  $\kappa\sigma^2$  as a function of the baryon chemical potential in the PNJL model along three freeze-out lines and comparing with BES-I measurement.

The same as in the NJL model, the peak structure of  $\kappa\sigma^2$  along the freeze-out line in the PNJL model is solely related to the CEP mountain, when the freeze-out line crosses the CEP mountain or crosses the foot of the CEP mountain, there will be a peak showing up for  $\kappa\sigma^2$ , and the location of the peak is related to the location of the CEP mountain. If there is no CEP,  $\kappa\sigma^2$  keeps flat in almost the whole chemical potential region. In the PNJL-1 and PNJL-2 models with the existence of CEP in the phase diagram, it is found that for both the first and second cases of the freeze-out lines, one can observe the dip-peak structure for  $\kappa\sigma^2$  along the freeze-out lines. The difference lies in that for the first freeze-out line case,  $\kappa\sigma^2$  goes to negative at the dip, and for the second freeze-out line case,  $\kappa\sigma^2$  is positive at the dip. This is because that for the first case, the freeze-out line starts from the back ridge of the chiral phase boundary and goes through the negative region of  $\kappa\sigma^2$ , then crosses the foot of the CEP mountain, therefore,  $\kappa\sigma^2$  decreases from around 0.1 and then down to negative value then rises up quickly and shows up a high peak around the critical chemical potential, thus shows a dip and then a peak structure of  $\kappa\sigma^2$  along the freeze-out line. For the second case, the freeze-out line starts from the back ridge of the deconfinement phase boundary, and has no chance to go through the negative region, then crosses the foot of the CEP mountain, though we can observe a dip structure but the magnitude of  $\kappa\sigma^2$  at the dip is positive. For the third case when the freeze-out line is far away from the phase boundary,  $\kappa\sigma^2$  along the freeze-out line is almost flat.

It is noticed that in the PNJL-1 model,  $\kappa\sigma^2$  along the second cases of freeze-out line shows a dip structure and a peak structure, and agrees well with the BES-I measurement. In the PNJL-3 model, there is no CEP in the phase diagram, and no special structure of  $\kappa\sigma^2$  along the freeze-out lines is observed.

#### E. The kurtosis of the baryon number fluctuation $\kappa \sigma^2$ in the $\mu$ PNJL model

In Fig. 6, we show the 3D plot for the kurtosis of baryon number fluctuation  $\kappa\sigma^2$  as a function of the temperature and baryon chemical potential in the  $\mu$ PNJL model. In Fig.7 we show the phase transition lines and 2D plot for  $\kappa\sigma^2$  as a function of the baryon chemical potential along different freeze-out lines for  $\mu$ PNJL-1 and  $\mu$ PNJL-2 models, respectively.

Same as that in the PNJL model, in the  $\mu$ PNJL model, there also exist two separate phase transitions for the chiral phase transition and deconfinement phase transition, and the deconfinement phase transition line also lays below the chiral phase transition line at small chemical potential region. From the 3D plot Fig.6 one can observe two separate phase boundaries at small baryon chemical potentials. The height of the ridge along the deconfinement phase boundary is around 2 at small chemical potentials in the  $\mu$ PNJL model, which is higher than that in the PNJL

model.

Similar to that in the PNJL model, we choose three different freeze-out lines: 1) Starting from the back ridge of the chiral phase boundary, goes through the negative region and then crosses the foot of the CEP mountain; 2) Starting from the back ridge of the deconfinement phase boundary, and then crosses the foot of the CEP mountain; 3) Starting from the front ridge of the deconfinement phase boundary and keeps far away from the CEP mountain. These three different freeze-out lines are indicated by long dashed, dashed-dotted and dashed lines, respectively. The structure of  $\kappa\sigma^2$  along the freeze-out line in  $\mu$ PNJL-1 and  $\mu$ PNJL-2 can show the dip and peak structure for both the first and second cases of the freeze-out lines,  $\kappa\sigma^2$  goes to negative at the dip in the first case, and keeps positive at the dip for the second freeze-out line case.

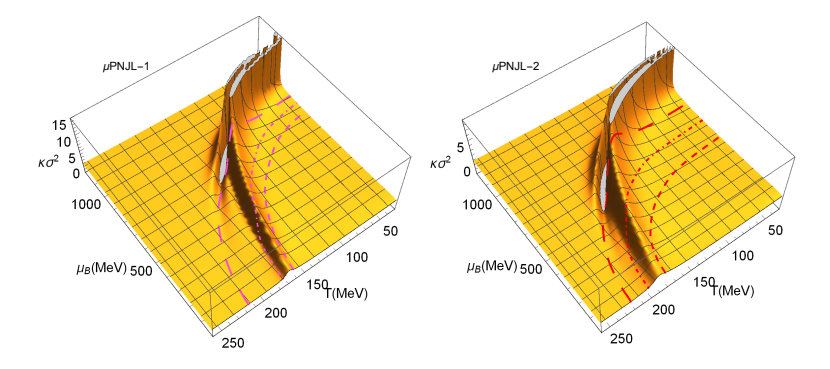


FIG. 6: The 3D plot for the kurtosis of baryon number fluctuation  $\kappa \sigma^2$  as a function of the temperature and baryon chemical potential in the  $\mu$ PNJL model.

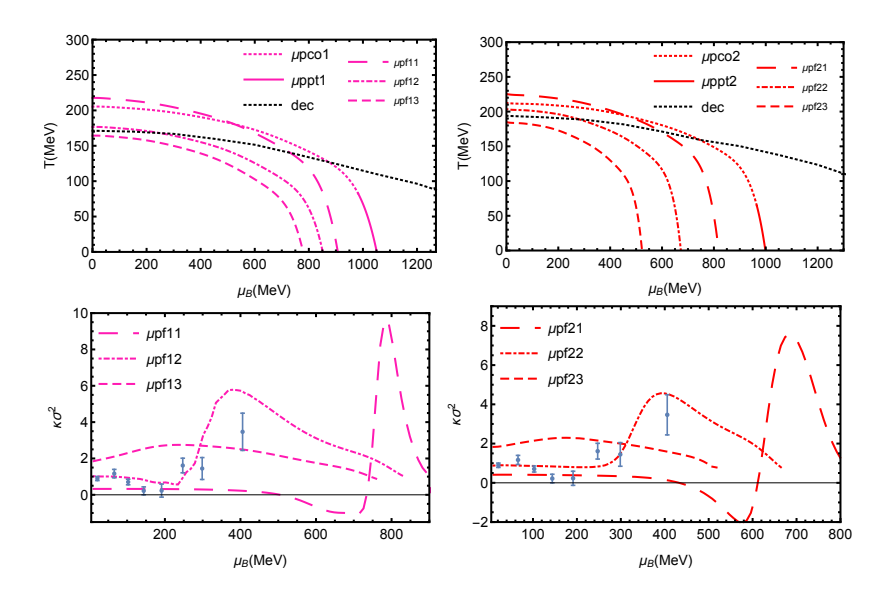


FIG. 7: (Above) The chiral phase transition line in the  $\mu$ PNJL model and three different freeze-out lines: 1) Starting from the back ridge of the chiral phase boundary, goes through the negative region and then crosses the foot of the CEP mountain; 2) Starting from the back ridge of the deconfinement phase boundary, and then crosses the foot of the CEP mountain; 3) Starting from the front ridge of the deconfinement phase boundary and keeps far away from the CEP mountain. These three different freeze-out lines are indicated by long dashed, dashed-dotted and dashed lines, respectively. (Below) The 2D plot for  $\kappa\sigma^2$  as a function of the baryon chemical potential in the  $\mu$ PNJL model along three freeze-out lines and comparing with BES-I measurement.

#### IV. CONCLUSION AND DISCUSSION

In this work, we have investigated the kurtosis  $\kappa \sigma^2$  of net baryon number fluctuation and analyze the formation of its dip and peak structures along the freeze out line in the NJL model, PNJL model as well as  $\mu$ PNJL model with

different parameter sets.

At zero chemical potential, the magnitude of  $\kappa\sigma^2$  is rather small in the NJL model comparing with lattice result, and it can reach around 1 in the PNJL model and 2 in the  $\mu$ PNJL model around the critical temperature. This indicates that the main contribution to the baryon number fluctuation comes from gluodynamics. It is noticed that in the PNJL model, the critical temperature for chiral phase transition is higher than that for deconfinement phase transition, i.e.  $T_0^{\chi} > T_0^D$ , and the value of  $\kappa\sigma^2$  at  $T_0^{\chi}$  is smaller than that at  $T_0^{D}$ . In some sense this agrees with lattice result, where the value of  $\kappa\sigma^2$  at  $T_0^{\chi}$  is smaller than that at  $T_0^{dec}$  describing an effective or physical confinement-deconfinement phase transition between quark matter and hadron matter. The temperature dependent  $\kappa\sigma^2$  is sensitive to the relation between the chiral and "deconfinement" phase transitions and can be used to constrain the model.

The peak structure of  $\kappa\sigma^2$  along the freeze-out line is solely determined by the existence of the CEP mountain. When the freeze-out line crosses the CEP mountain or crosses the foot of the CEP mountain, there will be a peak showing up for  $\kappa\sigma^2$  along the freeze-out line, and the location of the peak is close to the location of the CEP mountain. The higher the peak, the closer the peak location to the CEP. If the height of the peak is higher than 1, it is for sure that the freeze-out line crosses the foot of the CEP mountain, and if the height of the peak is higher than 15, then the freeze-out line should crosses the CEP mountain, and the peak location is almost the location of the CEP. In the case of no CEP, it is found that  $\kappa\sigma^2$  keeps flat almost in the whole chemical potential region and does not show any structure.

The formation of the dip structure is more complicated: Firstly, it requires the existence of the CEP in the QCD phase diagram; Secondly, it is sensitive to the relation between the freeze-out line and the phase boundary. The dip structure can be formed if the freeze-out line starts from the temperature above the critical temperature at  $\mu=0$  and crosses the phase boundary from above when the CEP exists in the phase diagram. Because the CEP is for chiral phase transition and there is a negative region of  $\kappa\sigma^2$  from the crossover side, if the freeze-out line starts from the back ridge of the chiral phase boundary and if it goes through the negative region of  $\kappa\sigma^2$ , and then crosses the CEP mountain or the foot of the CEP mountain, in this case one can observe a dip structure and a peak structure, and the magnitude of  $\kappa\sigma^2$  will go to negative at the dip. If the freeze-out line starts from the back ridge of the deconfinement phase boundary, and then crosses the foot of the CEP mountain, we can also see a dip and peak structure of  $\kappa\sigma^2$  along the freeze-out line, but the magnitude of  $\kappa\sigma^2$  will not go to negative at the dip. Therefore we can read the information on how does the freeze-out line crosses the chiral phase boundary from the negative/positive value at the dip of measured  $\kappa\sigma^2$  along the freeze-out line.

It is worthy mentioning that for the PNJL-1 with the freeze-out line starting from the back ridge of the deconfinement phase boundary and then crossing the foot of CEP mountain, the behavior of  $\kappa\sigma^2$  along the freeze-out line agree with the measurement of BES-I at RHIC. We show the relation between the freeze-out line and phase boundary for real QCD on the left and that in the PNJL-1 on the right in Fig.8. It is shown that indeed the extracted freeze-out temperature at BES-I [42] starts from the temperature above the critical temperature, and crosses the effective "deconfinement" transition line at about  $\mu_B = 400 \text{MeV}$ , where a peak is predicted to show up around.

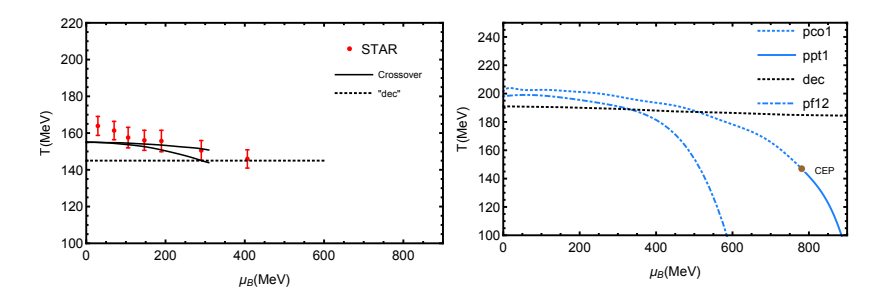


FIG. 8: (Left) The freeze-out temperatures determined by BES-I at RHIC (squres) [42], QCD phase boundary (solid lines) and the conjectured physical "deconfinement" phase transition between quark matter and hadron matter (dotted line). (Right) The freeze-out line, chiral phase transition line with existence of CEP and deconfinement phase transition line.

At last, we should mention that in this work, we didn't taken into account the non-thermal effect, memory effect [43–45], or finite size effect, which might play important roles to locate the CEP.

#### Acknowledgments

We thank valuable discussions with H.T.Ding, W.J.Fu, X.F.Luo and G.Y.Shao. M.H. acknowledges Aerospace Central Hospital where most part of the manuscript is written. This work is supported by the NSFC under Grant No. 11725523, 11735007 and 11261130311(CRC 110 by DFG and NSFC).

- [1] Z. Fodor and S. D. Katz, "A New method to study lattice QCD at finite temperature and chemical potential," *Phys. Lett.* **B534** (2002) 87–92, arXiv:hep-lat/0104001 [hep-lat].
- [2] H.-T. Ding, F. Karsch, and S. Mukherjee, "Thermodynamics of strong-interaction matter from Lattice QCD," Int. J. Mod. Phys. E24 no. 10, (2015) 1530007, arXiv:1504.05274 [hep-lat].
- [3] C. Schmidt and S. Sharma, "The phase structure of QCD," J. Phys. G44 no. 10, (2017) 104002, arXiv:1701.04707 [hep-lat].
- [4] R. D. Pisarski and F. Wilczek, "Remarks on the Chiral Phase Transition in Chromodynamics," Phys. Rev. D29 (1984) 338–341.
- [5] Y. Hatta and T. Ikeda, "Universality, the QCD critical / tricritical point and the quark number susceptibility," *Phys. Rev.* **D67** (2003) 014028, arXiv:hep-ph/0210284 [hep-ph].
- [6] T. M. Schwarz, S. P. Klevansky, and G. Papp, "The Phase diagram and bulk thermodynamical quantities in the NJL model at finite temperature and density," *Phys. Rev.* C60 (1999) 055205, arXiv:nucl-th/9903048 [nucl-th].
- [7] P. Zhuang, M. Huang, and Z. Yang, "Density effect on hadronization of a quark plasma," *Phys. Rev.* C62 (2000) 054901, arXiv:nucl-th/0008043 [nucl-th].
- [8] J.-W. Chen, J. Deng, and L. Labun, "Baryon susceptibilities, non-Gaussian moments, and the QCD critical point," *Phys. Rev.* **D92** no. 5, (2015) 054019, arXiv:1410.5454 [hep-ph].
- [9] J.-W. Chen, J. Deng, H. Kohyama, and L. Labun, "Robust characteristics of nongaussian fluctuations from the NJL model," *Phys. Rev.* **D93** no. 3, (2016) 034037, arXiv:1509.04968 [hep-ph].
- [10] W. Fan, X. Luo, and H.-S. Zong, "Mapping the QCD phase diagram with susceptibilities of conserved charges within NambuCJona-Lasinio model," Int. J. Mod. Phys. A32 no. 11, (2017) 1750061, arXiv:1608.07903 [hep-ph].
- [11] W. Fan, X. Luo, and H. Zong, "Identifying the presence of the critical end point in QCD phase diagram by higher order susceptibilities," arXiv:1702.08674 [hep-ph].
- [12] W.-j. Fu and Y.-l. Wu, "Fluctuations and Correlations of Conserved Charges near the QCD Critical Point," *Phys. Rev.* **D82** (2010) 074013, arXiv:1008.3684 [hep-ph].
- [13] E. S. Bowman and J. I. Kapusta, "Critical Points in the Linear Sigma Model with Quarks," Phys. Rev. C79 (2009) 015202, arXiv:0810.0042 [nucl-th].
- [14] H. Mao, J. Jin, and M. Huang, "Phase diagram and thermodynamics of the Polyakov linear sigma model with three quark flavors," J. Phys. G37 (2010) 035001, arXiv:0906.1324 [hep-ph].
- [15] B. J. Schaefer and M. Wagner, "QCD critical region and higher moments for three flavor models," *Phys. Rev.* D85 (2012) 034027, arXiv:1111.6871 [hep-ph].
- [16] B.-J. Schaefer and M. Wagner, "Higher-order ratios of baryon number cumulants," Central Eur. J. Phys. 10 (2012) 1326–1329, arXiv:1203.1883 [hep-ph].
- [17] S.-x. Qin, L. Chang, H. Chen, Y.-x. Liu, and C. D. Roberts, "Phase diagram and critical endpoint for strongly-interacting quarks," *Phys. Rev. Lett.* **106** (2011) 172301, arXiv:1011.2876 [nucl-th].
- [18] J. Luecker, C. S. Fischer, L. Fister, and J. M. Pawlowski, "Critical Point and Decon?nement from Dyson-Schwinger Equations," PoS CPOD2013 (2013) 057, arXiv:1308.4509 [hep-ph].
- [19] W.-j. Fu, J. M. Pawlowski, F. Rennecke, and B.-J. Schaefer, "Baryon number fluctuations at finite temperature and density," *Phys. Rev.* **D94** no. 11, (2016) 116020, arXiv:1608.04302 [hep-ph].
- [20] M. A. Stephanov, "Non-Gaussian fluctuations near the QCD critical point," Phys. Rev. Lett. 102 (2009) 032301, arXiv:0809.3450 [hep-ph].
- [21] M. A. Stephanov, "On the sign of kurtosis near the QCD critical point," Phys. Rev. Lett. 107 (2011) 052301, arXiv:1104.1627 [hep-ph].
- [22] M. Asakawa, S. Ejiri, and M. Kitazawa, "Third moments of conserved charges as probes of QCD phase structure," *Phys. Rev. Lett.* **103** (2009) 262301, arXiv:0904.2089 [nucl-th].
- [23] C. Athanasiou, K. Rajagopal, and M. Stephanov, "Using Higher Moments of Fluctuations and their Ratios in the Search for the QCD Critical Point," Phys. Rev. **D82** (2010) 074008, arXiv:1006.4636 [hep-ph].
- [24] R. Critelli, J. Noronha, J. Noronha-Hostler, I. Portillo, C. Ratti, and R. Rougemont, "Critical point in the phase diagram of primordial quark-gluon matter from black hole physics," Phys. Rev. D96 no. 9, (2017) 096026, arXiv:1706.00455 [nucl-th].
- [25] V. Vovchenko, J. Steinheimer, O. Philipsen, and H. Stoecker, "Cluster Expansion Model for QCD Baryon Number Fluctuations: No Phase Transition at  $\mu_B/T < \pi$ ," arXiv:1711.01261 [hep-ph].
- [26] STAR Collaboration, L. Adamczyk *et al.*, "Energy Dependence of Moments of Net-proton Multiplicity Distributions at RHIC," *Phys. Rev. Lett.* **112** (2014) 032302, arXiv:1309.5681 [nucl-ex].
- [27] STAR Collaboration, M. M. Aggarwal et al., "Higher Moments of Net-proton Multiplicity Distributions at RHIC," Phys.

- Rev. Lett. 105 (2010) 022302, arXiv:1004.4959 [nucl-ex].
- [28] X. Luo and N. Xu, "Search for the QCD Critical Point with Fluctuations of Conserved Quantities in Relativistic Heavy-Ion Collisions at RHIC: An Overview," Nucl. Sci. Tech. 28 no. 8, (2017) 112, arXiv:1701.02105 [nucl-ex].
- [29] Z. Li, Y. Chen, D. Li, and M. Huang, "Locating the QCD critical end point through the peaked baryon number susceptibilities along the freeze-out line," Chin. Phys. C42 no. 1, (2018) 013103, arXiv:1706.02238 [hep-ph].
- [30] Y. Nambu and G. Jona-Lasinio, "Dynamical Model of Elementary Particles Based on an Analogy with Superconductivity. 1.," Phys. Rev. 122 (1961) 345–358.
- [31] Y. Nambu and G. Jona-Lasinio, "DYNAMICAL MODEL OF ELEMENTARY PARTICLES BASED ON AN ANALOGY WITH SUPERCONDUCTIVITY. II," *Phys. Rev.* **124** (1961) 246–254.
- [32] S. P. Klevansky, "The Nambu-Jona-Lasinio model of quantum chromodynamics," Rev. Mod. Phys. 64 (1992) 649-708.
- [33] K. Fukushima, "Phase diagrams in the three-flavor Nambu-Jona-Lasinio model with the Polyakov loop," *Phys. Rev.* D77 (2008) 114028, arXiv:0803.3318 [hep-ph]. [Erratum: Phys. Rev.D78,039902(2008)].
- [34] N. Weiss, "The Effective Potential for the Order Parameter of Gauge Theories at Finite Temperature," Phys. Rev. **D24** (1981) 475.
- [35] C. Ratti, S. Roessner, M. A. Thaler, and W. Weise, "Thermodynamics of the PNJL model," Eur. Phys. J. C49 (2007) 213-217, arXiv:hep-ph/0609218 [hep-ph].
- [36] G.-y. Shao, Z.-d. Tang, X.-y. Gao, and W.-b. He, "Baryon number fluctuations and QCD phase structure," arXiv:1708.04888 [hep-ph].
- [37] B.-J. Schaefer, J. M. Pawlowski, and J. Wambach, "The Phase Structure of the Polyakov-Quark-Meson Model," Phys. Rev. D76 (2007) 074023, arXiv:0704.3234 [hep-ph].
- [38] X.-y. Xin, S.-x. Qin, and Y.-x. Liu, "Improvement on the PolyakovCNambuCJona-Lasinio model and the QCD phase transitions," *Phys. Rev.* **D89** no. 9, (2014) 094012.
- [39] G.-y. Shao, Z.-d. Tang, M. Di Toro, M. Colonna, X.-y. Gao, and N. Gao, "Phase transition of strongly interacting matter with a chemical potential dependent Polyakov loop potential," *Phys. Rev.* D94 no. 1, (2016) 014008, arXiv:1603.09033 [nucl-th].
- [40] M. Dutra, O. Louren?o, A. Delfino, T. Frederico, and M. Malheiro, "PolyakovCNambuCJona-Lasinio phase diagrams and quarkyonic phase from order parameters," *Phys. Rev.* **D88** no. 11, (2013) 114013, arXiv:1312.1130 [hep-ph].
- [41] A. Bazavov et al., "The QCD Equation of State to  $\mathcal{O}(\mu_B^6)$  from Lattice QCD," Phys. Rev. **D95** no. 5, (2017) 054504, arXiv:1701.04325 [hep-lat].
- [42] STAR Collaboration, S. Das, "Identified particle production and freeze-out properties in heavy-ion collisions at RHIC Beam Energy Scan program," arXiv:1412.0499 [nucl-ex]. [EPJ Web Conf.90,08007(2015)].
- [43] S. Mukherjee, R. Venugopalan, and Y. Yin, "Real time evolution of non-Gaussian cumulants in the QCD critical regime," *Phys. Rev.* C92 no. 3, (2015) 034912, arXiv:1506.00645 [hep-ph].
- [44] S. Mukherjee, R. Venugopalan, and Y. Yin, "Universal off-equilibrium scaling of critical cumulants in the QCD phase diagram," *Phys. Rev. Lett.* **117** no. 22, (2016) 222301, arXiv:1605.09341 [hep-ph].
- [45] L. Jiang, P. Li, and H. Song, "Correlated fluctuations near the QCD critical point," Phys. Rev. C94 no. 2, (2016) 024918, arXiv:1512.06164 [nucl-th].